Low cycle fatigue of 316L stainless steel processed by surface mechanical attrition treatment (SMAT)

Zhidan Sun[1], *Jianqiang* Zhou[1], *Delphine* Retraint[1,*], *Thierry* Baudin[2], *Anne-Laure* Helbert[2], *François* Brisset[2], and *Pascale* Kanouté[1,3]

[1]ICD, P2MN, LASMIS, University of Technology of Troyes, CNRS, Troyes, France
[2]ICMMO - UMR 8182, Université Paris-Sud, 91405 Orsay, France
[3]ONERA, The French Aerospace Lab, 29 avenue de la Division Leclerc, 92322 Chatillon Cedex, France

Abstract. In this work, the effect of surface mechanical attrition treatment (SMAT) on the cyclic behaviour of a 316L stainless steel under low cycle fatigue (LCF) is investigated. The LCF results are presented in the form of cyclic stress amplitude evolution for both untreated and SMATed samples. In order to better understand the microstructure change due to cyclic loading, electron backscatter diffraction (EBSD) is used to characterize the microstructure of the SMATed samples before and after fatigue tests. A microstructure gradient is highlighted for samples after SMAT from the top surface layer in nanocrystalline grains to the interior region non-affected by impacts. Under LCF loading, new slip systems are activated in the work hardened region, whereas no plastic slip is activated in the nanostructured layer. The residual stresses generated by SMAT are measured using X-ray diffraction (XRD), and their relaxations under cyclic loading are studied by taking into account the microstructure change. The cyclic behaviour of the samples in different material states is interpreted based on these investigations.

1 Introduction

Fatigue properties of metallic materials are important for design and life prediction of mechanical components subjected to cyclic loading in service. It is well known that the fatigue properties of materials are sensitive to grain size as well as residual stresses. Small grains can effectively increase the yield strength of a material and consequently enhance its fatigue crack initiation resistance [1, 2], whereas coarse grains exhibit better crack propagation resistance due to the good ductility and toughness of materials. Since most fatigue cracks initiate from the surface and propagate to the interior of a structure, a component with a nanostructured surface layer and an inner coarse grained matrix can have improved fatigue resistance [3]. Furthermore, the presence of compressive residual stress is beneficial for fatigue life improvement through increasing the resistance to both crack initiation and propagation.

Surface mechanical attrition treatment (SMAT) is a surface treatment technique which can transform the coarse grained surface layer of a material into nanosized grains by means of severe plastic deformation (SPD) [4-6]. SMAT is based on mechanical impacts on the surface of a structure by metallic balls with high kinetic energy. This technique is able to generate a large quantity of crystallographic defects such as dislocations, deformation twins, which can lead to the formation of refined grains down to the nanometer scale at the surface. The obtained nanostructured layer coupled with compressive residual stresses generated by SMAT can effectively improve the fatigue strength of materials [7]. To promote SMAT for example in engineering applications, it is important to have a good understanding of all the properties of materials processed by this technique including fatigue properties. It has been experimentally demonstrated that SMAT can significantly improve the fatigue resistance of metallic materials [5, 8-10]. On the one hand, the near surface compressive residual stresses can improve fatigue life by increasing the resistance to crack initiation and propagation. On the other hand, a work hardened layer generated by mechanical impacts can enhance the material strength by increasing for example the elastic limit [11, 12]. In addition, in the case of SMAT, the presence of a superficial nanostructured layer can effectively increase the yield strength and consequently enhance the materials' fatigue crack initiation resistance [8]. However, most of the studies performed in the literature concerning the effect of SMAT on fatigue properties were performed in high cycle fatigue (HCF) regime [5, 13-16]. It is well documented that the residual stress relaxation is strongly dependent on load amplitude. When shot peened samples are subjected to high strain/stress amplitudes, the generated compressive residual stresses can be quickly relaxed, i.e. during the first several cycles [16-18].

In this work, low cycle fatigue (LCF) behaviour of a SMATed 316L stainless steel is investigated compared to its untreated state. Electron backscatter diffraction (EBSD) observation and microhardness test are conducted to characterize the SMAT affected region before and after fatigue test. The effect of SMAT on the mechanical behaviour of this material under cyclic loading is analysed. A comparison between SMATed and untreated samples is given based on the results including cyclic stress amplitude evolution, cyclic hardening/softening behaviour, and hysteresis loop. The results are discussed through analysing the eventual

* Corresponding author: delphine.retraint@utt.fr

microstructure change and residual stress relaxation due to cyclic loading.

2 Material and experimental procedures

The material used in this work is a biomedical grade 316L ASTM F138 austenitic stainless steel. Its chemical composition is given as follows (wt.%): 17.37Cr, 14.52Ni, 1.7Mn, 2.8Mo, 0.26Si, 0.013C, 0.017P, 0.08Cu, 0.003S, 0.07V, 0.088N, <0.005Ti, and balance with Fe. The as-received material has an initial average grain size of about 15 µm. For fatigue tests, dumbbell shape samples with an overall length of 110 mm were used. The parallel length of the reduced section is 12 mm with a diameter of 6 mm. SMAT was carried out so as to cover the entire parallel length of the reduced section. SMAT is based on the projection of spherical shots (3 mm diameter) boosted by a high frequency (20 kHz) ultrasonic generator. More detailed description of SMAT can be found in the literature [4]. In this work, the SMAT conditions used corresponds to a treatment of 15 minutes with a generator power of 30%, followed by a treatment of 5 minutes with a generator power of 50%.

LCF tests were conducted with untreated (UNT) and SMATed samples at room temperature using a servo-hydraulic machine. Uniaxial tension-compression fatigue tests were performed under total strain control with a load ratio of $R_\varepsilon = -1$. An extensometer with a gauge length of 10 mm was used to control the total strain, and a strain rate of $4 \times 10^{-3} s^{-1}$ was applied for all the fatigue tests. When the stress amplitude drop reached 30%, the samples were considered failed and the fatigue tests were stopped.

Residual stress was measured on the SMATed samples before and after fatigue tests by X-ray diffraction (XRD) with a Cr-Kα radiation using classical $\sin^2\psi$ method. To determine the in-depth residual stress variation, iterative electrolytic polishing was used to remove material from the surface of samples. Subsequent XRD measurements were performed in order to plot in-depth residual stress variation curve for the SMATed samples before and after fatigue tests in order to study the residual stress relaxation.

3 Microstructure and hardness

3.1 Microstructure observation

EBSD observation on transverse cross-section reveals a microstructure gradient in the SMAT affected region, as illustrated in Fig. 1. It can be seen that the severe plastic deformation induced by the impingement of shots flying at high speed generated a refinement of coarse grains down to nanometer scale in the top surface layer (Fig. 1b). The depth of the nanostructured layer is about 5 µm, followed by a transition region in which the grains are plastically deformed by impacts during SMAT. In this work hardened region, the impact intensity is actually lower than in the top surface nanostructured layer, and thus only many plastic slips have been activated without the formation of small grains. This is because the grain refinement requires not only a high accumulated plastic strain but also a high strain rate. In the region far from the top surface, both the accumulated plastic strain and the strain rate are significantly reduced. In the work hardened region, the grains are subdivided by transgranular traces which correspond to plastic slips activated by multi-directional impacts of shots during SMAT. Notice that there are few deformation-induced twins in the SMAT affected region including the nanostructured layer and the work hardened region [19].

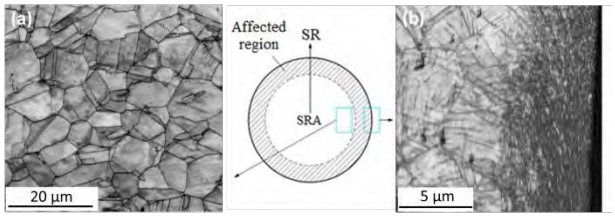

Figure 1. Typical transverse cross-sectional EBSD micrographs showing typical regions of different microstructures for a sample treated by SMAT: (a) non-affected interior region, and (b) SMAT affected region including the nanostructured layer and a part of the work hardened region.

3.2 Hardness measurement

Microhardness was measured to assess the change of mechanical strength in the SMAT affected region, as frequently done in the literature [4, 20, 21]. Fig. 2 presents the in-depth hardness variation from the treated surface for a SMATed sample. The microhardness was also measured for an untreated sample and its variation was plotted in Fig. 2 for comparison. The hardness was determined by using a Vickers microhardness tester, with a load of 0.025 kg. From the hardness variation curves shown in Fig. 2, it can be seen that there is a significant hardness increase in the SMAT affected region with respect to the untreated sample. Close to the treated surface, the hardness reaches a value as high as 400 HV0.025 which is about twice that in the central non-affected region of the sample. The hardness remains almost constant between 0.5 mm and 2 mm below the treated surface. This signifies that the depth within which the material is affected by SMAT is at least 500 µm. Fig. 2 also shows that in the interior region, the microhardness is obviously higher for the untreated sample than for the SMATed sample. It means that there is a decrease of hardness in the interior region caused by SMAT. However, as observed by EBSD, beyond the depth of about 500 µm, there is almost no plastic slip. Therefore, this decrease of hardness could be due to the presence of tensile residual stress in the interior region. Notice that the existence of tensile residual stress in the interior region is needed to compensate for the compressive residual stress present in the near surface region. The residual stress in-depth variation will be presented after in this paper.

4 Cyclic behaviour

4.1 Cyclic stress amplitude

Cyclic stress amplitude evolution during cyclic loading gives a good description of the cyclic behaviour of

materials in terms of hardening/softening as function of the number of cycles. The hardening/softening behaviour of a material can be altered by mechanical surface treatment techniques such as SMAT.

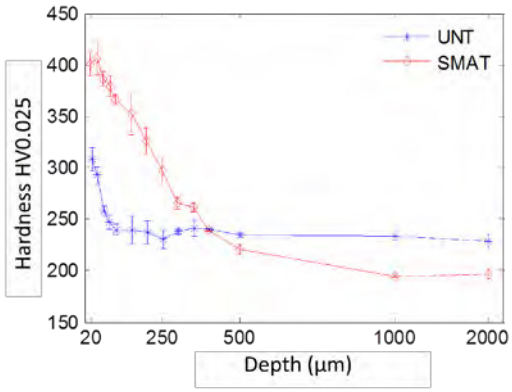

Figure 2. In-depth hardness variations from the top surface for untreated (UNT) and SMATed samples.

Fig. 3 shows the cyclic stress amplitude evolution with the increase of the number of cycles for untreated and SMATed samples obtained under different total strain amplitudes from ±0.3% to ±1.25%. Different strain amplitude levels were used in order to discern the eventual load amplitude dependent behaviour of the material. Globally it can be observed, by comparing Fig. 3a and Fig. 3b, that SMAT significantly enhanced the mechanical strength and changed the cyclic hardening/softening behaviour of the samples. From Fig. 3, it can also be seen that higher imposed strain amplitude gives higher cyclic stress amplitude. Furthermore, for a given strain amplitude, the cyclic stress amplitudes of the SMATed samples are obviously higher than that of the untreated ones.

The hardening/softening behaviour (characterized by the stress increase/decrease with respect to the initial state) of the material throughout fatigue tests can also be observed from the curves shown in Fig. 3. At the beginning of cyclic loading, there is an increase of stress amplitude during the first several cycles, which corresponds to the initial hardening of the material. It can be distinguished that under lower strain amplitude (±0.3% for example), the maximum stress amplitude is reached earlier, and there is an evident longer softening phase which follows the short period of initial hardening. Under strain amplitude of ±1.25%, untreated samples undergo more obvious initial hardening than the SMATed samples. In addition, the phenomenon of secondary hardening which follows the cyclic softening period can be observed for untreated samples under high strain amplitude (±1.25% and ±0.8%). In the case of low strain amplitude (±0.5% and ±0.3%), the secondary hardening is not present, and the samples undergo long term period softening. For the SMATed samples, the stress amplitude is nearly stabilized by the end of the fatigue tests under high stress amplitudes (±0.8% and ±1.25%), while under low strain amplitudes (±0.3% and ±0.5%), only the long term softening period is present (Fig. 3b).

The change of cyclic behaviour of the SMATed samples with respect to the untreated ones is due to the SMAT affected region which generally enhances the global mechanical strength of the SMATed samples under monotonic loading [4, 20, 21]. In this paper, the strengthening effect of shot impacts is manifested by the increase of the global stress level induced by SMAT, as shown in Fig. 3. On the one hand, strain hardening induced by shot impacts can improve the mechanical strength due to dislocation entanglement which can impede permanent deformation of the material during subsequent cyclic loading. On the other hand, the generated nanostructured layer has much higher yield strength than its initial non-treated state according to Hall-Petch relationship. However, the nanostructured layer might have a small contribution to the global mechanical behaviour of the samples because of its very thin thickness (5 µm) compared to the depth of the work hardened region (more than 500 µm according to the microhardness curves) and the diameter of the sample (6 mm).

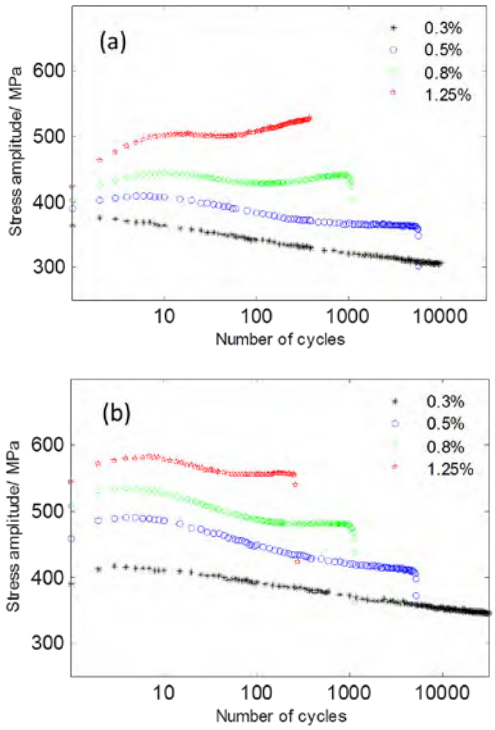

Figure 3. Cyclic stress amplitude evolution curves obtained under different strain amplitudes for: (a) untreated samples, and (b) SMATed samples.

In addition, as presented above, the interior region of the SMATed samples has no plastic deformation. The interior region should also undergo the cyclic secondary hardening as undergone by untreated samples (Fig. 3a). This implies that the disappearance of secondary hardening for SMATed samples under high strain amplitude is related to the SMAT affected region. Therefore, this SMAT affected region should exhibit cyclic softening behaviour, which allows to reduce the secondary hardening effect of the interior region on the whole SMATed sample.

4.2. Hysteresis loops

LCF hysteresis loop describes the relationship between strain and stress during one cycle, and characterizes more specifically the plastic cyclic deformation behaviour of materials. Fig. 4 illustrates the comparison of hysteresis loops for the untreated and SMATed samples under different strain amplitudes at different number of cycles. It can be seen that at the 2nd cycle the hysteresis loops of SMATed samples have larger height and smaller width (which represents plastic strain range) than untreated samples, under both high (Fig. 4a) and low (Fig. 4b) strain amplitudes. This means that the SMATed samples exhibit higher stress amplitude and lower plastic strain at the beginning of cyclic loading. As cyclic loading continues, the difference between these hysteresis loops obtained with different material states gradually decreases, and they tend to become superposed by the end of fatigue tests, especially under high strain amplitude (see the two dotted curved presented in Fig. 4a obtained at 260th cycle). This result implies that SMAT mainly affects the cyclic behaviour during the early stage of cyclic loading, and its effect is gradually reduced with the increase of the number of cycles.

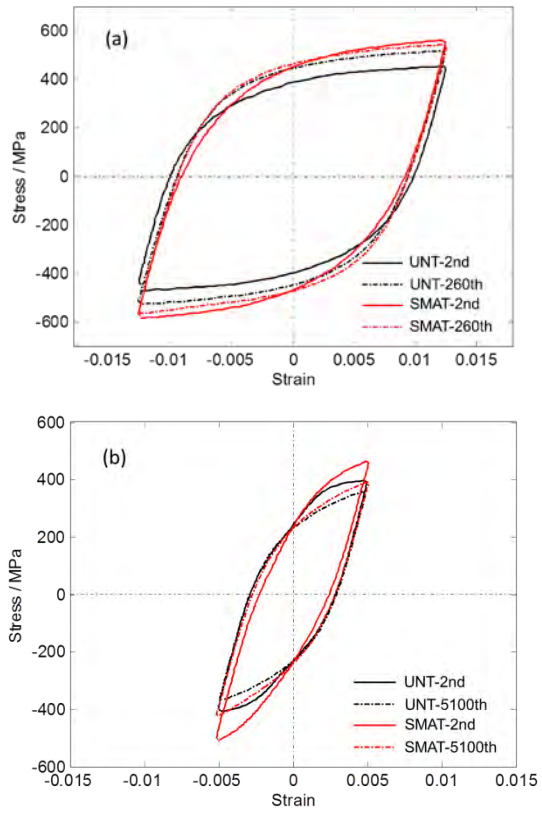

Figure 4. Hysteresis loops obtained with the untreated and SMATed samples at the beginning of fatigue tests (2nd cycle) and by the end of fatigue tests (260th cycle) under strain amplitude of (a) ±1.25% and (b) ±0.5%.

Other information which can be obtained from Fig. 4 concerns the hardening/softening. Under high strain amplitude (±1.25%), comparing the hysteresis curves obtained at 2nd and 260th cycles, it can be seen that the untreated sample undergoes cyclic hardening, whereas the SMATed sample undergoes a slight cyclic softening (Fig. 4a). In contrast, under low strain amplitude (±0.5%), both the untreated and the SMATed samples undergo softening, through comparing the hysteresis curves obtained at 2nd and 5100th cycles (Fig. 4b). These observed hardening/softening phenomena are consistent with the analysis given in Section 4.1 regarding the stress amplitude evolution.

5 Analysis and discussion

The in-depth hardness variation of SMATed samples after fatigue tests was measured in order to reveal the change in material properties. Fig. 5 shows an example of results obtained with strain amplitude of ±1.25%. It can be seen that after fatigue loading, compared to the state without fatigue, the hardness in the work hardened region of the SMATed sample decreases about 50 HV0.025, whereas the hardness in the interior region increases from 200 HV0.025 to about 230 HV0.025. This means that the work hardened region of the SMATed sample is softened, and the interior region (which also represents the untreated state of material) is hardened due to fatigue loading, with respect to their initial states. This investigation is consistent with the result presented in Fig. 3 in which it is shown that untreated samples underwent cyclic hardening under high strain amplitudes (Fig. 3a). By contrast, the cyclic hardening under high strain amplitude illustrated in Fig. 3b is less pronounced for the SMATed samples. This must be due to the cyclic softening of the work hardened region, as revealed by the hardness measurement shown in Fig. 5.

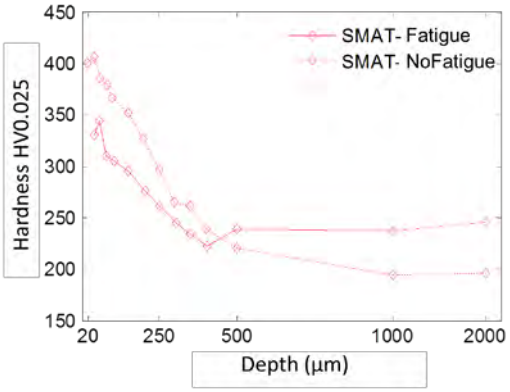

Figure 5. In-depth hardness variation from the treated surface for a SMATed sample after fatigue. The curve for a sample after SMAT (without fatigue) is also given for comparison.

It is worth mentioning that the residual stress could also have a contribution to the hardness change, as indicated above. If the tensile residual stress in the interior region has been (partially) relaxed during cyclic loading due to plastic deformation, it could also lead to an increase of hardness. According to the measurement of residual stress with DRX, it seems that this assumption could be confirmed. Fig. 6 illustrates the in-depth longitudinal residual stress variation for SMATed samples before and after fatigue tests with different strain amplitudes (±0.5% and ±1.25%). It can be seen that under stain amplitude of ±1.25%, nearly most residual stress is relaxed by the end of fatigue test, whereas under ±0.5%, the residual stress is partially

relaxed and remains equal to about 30% of the initial residual stress generated by SMAT.

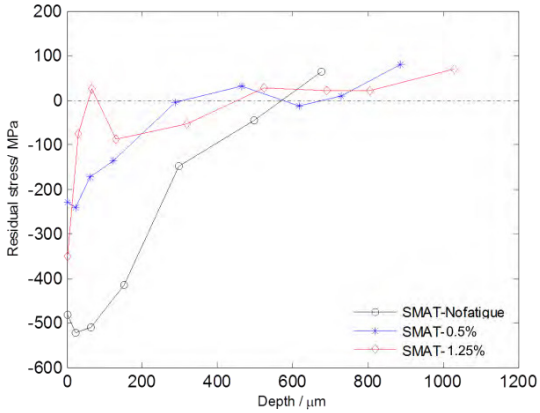

Figure 6. In-depth longitudinal residual stress variation for SMATed samples showing residual stress relaxation due to cyclic loading with different strain amplitudes. The curve obtained with the SMATed sample without fatigue is also given for comparison.

For fatigue tests, particular attention was paid to the eventual microstructure evolution of the SMAT affected region including the nanostructured layer and the work hardened (or plastically deformed) region. The results show that no obvious difference in grain size distribution can be noticed in the interior region for the samples before and after fatigue tests. This means that no grain size modification occurred in this region due to fatigue loading. However, according to Fig. 7, in all the regions except the nanostructured layer (Fig. 7a), grain orientation spread (GOS) has been increased under the effect of cyclic fatigue loading (Figs. 7b and 7c), with respect to the material state just obtained by SMAT. Notice that GOS characterizes the mean intragranular misorientation, i.e. the misorientation within a grain. Thus the GOS changes shown in Figs. 7b and 7c must be due to the plastic deformation activated by fatigue loading. This point of view is consistent with the literature. As indicated in [22], the plastic deformation in polycrystalline materials is able to generate intragranular disorientation, and accordingly an increase of GOS.

Fig. 8 shows the plastic slip traces present in the work hardened region of the SMATed samples before and after fatigue tests observed by EBSD. As already described above, SMAT induced plastic slips due to shot impacts (Fig. 1b and Fig. 8a). During the subsequent fatigue loading, the slip plane trace density is increased (Fig. 8b). Note that the hardening/softening behaviour as well as the residual stress relaxation is strongly related to the plastic slip activities due to fatigue loading. The red crosses shown in Fig. 8 indicate the planes {111} of the activated systems which are confirmed to be {111} <110> in this study. As a matter of fact, plastic slips newly activated by fatigue loading can further split the grains and consequently increase the intragranular disorientation inside each grain. This investigation is in good agreement with the GOS distribution presented in Fig. 7.

However, in the nanostructured layer, no change of GOS was caused by fatigue loading (Fig. 7a), which means that there is almost no plastic slip activated by cyclic loading in this area. This could be due to the fact that the yield stress of the nanostructured layer (with nanoscale grain size) is much higher than that of the work hardened layer or the interior non-affected region of the sample where the grains have an ordinary size. It is well known that the grain interior slip resistance increases with the decrease of grain size. The activation of plastic slips is thus more difficult in the nanostructured layer, which is consistent with the previous results on the mechanical behaviour of nanocrystalline or ultra-fine grained materials reported in the literature [23-25].

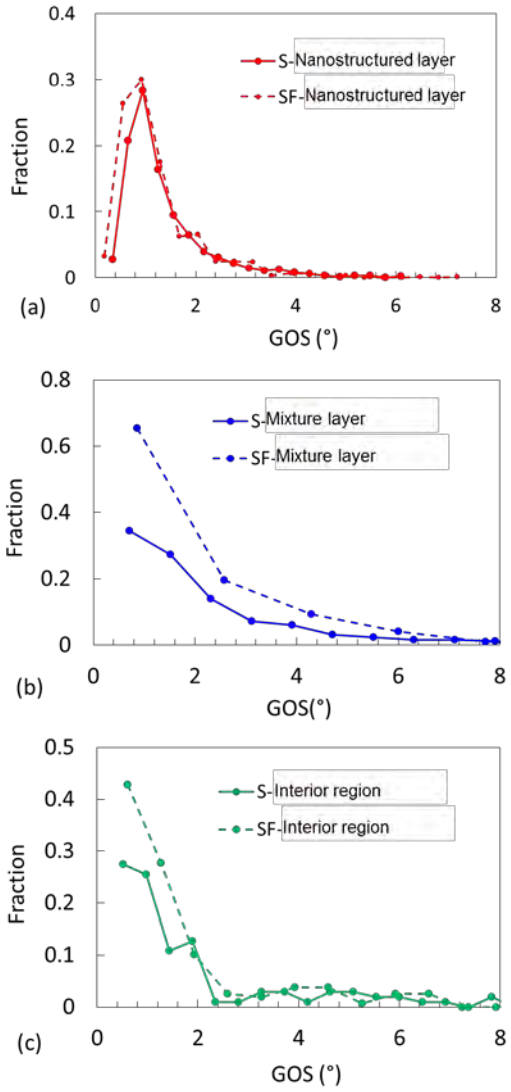

Figure 7 – GOS distribution calculated in different areas: (a) nanostructured layer, (b) work hardened region, and (c) interior region, for SMATed state (S) as well as SMATed and fatigued state (SF).

Furthermore, under cyclic loading with high strain amplitude, as indicated above, new plastic slips can be activated, which could lead to the restructuring of the dislocations introduced by SMAT in the work hardened region. As cyclic loading continues, the dislocation structure in the work hardened region induced by SMAT could tend to become similar to that in non-affected region of the sample. This constitutes the reason that the two curves corresponding to the untreated and SMATed

samples tend to be superposed by the end of fatigue tests (Fig. 4a). In addition, accompanied by these dislocation activities, most of the compressive residual stresses introduced by SMAT are relaxed, especially during the first several cycles under high strain amplitude [16], and the remained compressive residual stresses may not be high enough to significantly influence the fatigue properties at later stage of fatigue tests. This investigation concerning residual stress relaxation has been confirmed by the residual stress measurement using XRD, as shown in Fig. 6.

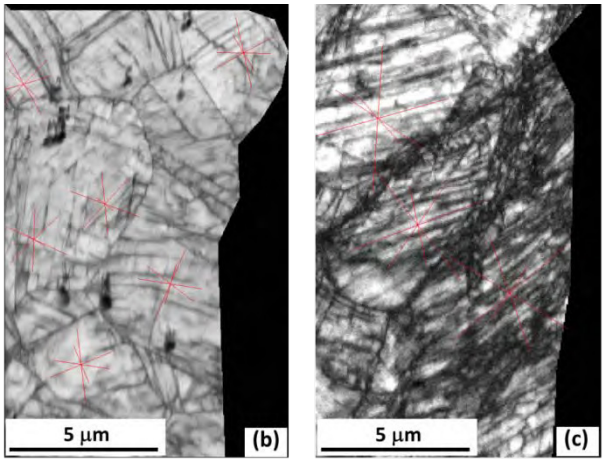

Figure 8 – Image quality (IQ) maps illustrating (a) the presence of plastic slip traces in the work hardened area without fatigue, and (b) the state of plastic slips in the work hardened area of a SMATed sample after fatigue. {111} plane traces are indicated by red crosses [19].

6 Conclusions

In this work, the effect of SMAT on low cycle fatigue behaviour of a 316L austenitic stainless steel was investigated, and the following conclusions can be drawn:

(1) After SMAT, a microstructure gradient is generated in the SMAT affected region, from the nanostructured layer to the non-affected bulk of the sample, through the transition region where many plastic slips are present.

(2) Cyclic stress amplitude of SMATed samples is enhanced due to higher strength of the SMAT affected region. During cyclic loading, the SMAT affected region undergoes cyclic softening, whereas the non-affected interior region is hardened under high strain amplitude (±1.25%), and softened under low strain amplitude (±0.5%).

(3) Comparison of hysteresis loops between different cycle numbers (at the beginning and by the end of fatigue tests) indicates that SMAT mainly affects the cyclic behaviour of the studied material in the early stage of fatigue test, and this effect is gradually attenuated as cyclic loading goes on.

(4) Under the effect of fatigue loading, new plastic slips are activated in the work hardened region, which accordingly leads to an increase of GOS. However, in the nanostructured layer, no obvious change of GOS can be observed. This could be due to the fact that the slip resistance is higher in the nanocrystalline or ultra-fine materials.

Acknowledgements

This work was supported by the Champagne-Ardenne Research Council through NANOSURF and NANOTRIBO projects with grateful acknowledgement.. It is also a pleasure to acknowledge the University of Technology of Troyes, Grand Troyes and Conseil Départemental de l'Aube for financial support through CompNano project. J. Zhou acknowledges the MESR for the financial support of his PhD.

References

1 T. Hanlon, Y.N. Kwon, S. Suresh, Scripta Mater. **49**, 675 (2003).
2 L. Yang, N.R. Tao, K. Lu, L. Lu, Scripta Mater. **68**, 801 (2013).
3 Y. Li, L. Zhou, W. He, G. He, X. Wang, X. Nie, B. Wang, S. Luo, Y. Li, Sci. Technol. Adv. Mater. **14**, 055010 (2013).
4 K. Lu, J. Lu, Mater. Sci. Eng. A 375-377, 38 (2004).
5 T. Roland, D. Retraint, K. Lu, J. Lu, Scripta Mater. **54**, 1949 (2006).
6 Y. Pi, G. Agoda, S. Potiron, C. Demangel, D. Retraint, H. Benhayoune, J. Nanosci. Nanotechnol. **12**, 4892 (2012).
7 T. Roland, D. Retraint. K. Lu, J. Lu, Mater. Sci. Forum **490-491**, 625 (2005).
8 H.A. Padilla, B.L. Boyce, Exp. Mech. **50**, 5 (2010).
9 T. Hanlon, E.D. Tabachnikova, S. Suresh, Fatigue Damage Struct. Mater. V **27**, 1147 (2005).
10 K.A. Gujba, M. Medraj, Materials 7, 7925 (2014).
11 J. Zhou, Z. Sun, P. Kanouté, D. Retraint, Int. J. Fatigue **103**, 309 (2017).
12 K. Dalaei, B. Karlsson, L-E. Svensson, Mater. Sci. Eng. A **528**, 1008 (2011).
13 J.C. Villegas, L.L. Shaw, K. Dai, W. Yuan, J. Tian, P.K. Liaw, D.L. Klarstrom, Philos. Mag. Lett. **85**, 427, (2005).
14 D. Li, H.N. Chen, H. Xu, Appl. Surf. Sci. **255**, 3811 (2009).
15 L.L. Shaw, J.W. Tian, A.L. Ortiz, K. Dai, J.C. Villegas, P.K. Liaw, R. Ren, D.L. Klarstrom, Mater. Sci. Eng. A **527**, 986 (2010).
16 K. Dalaei, B. Karlsson, Int. J. Fatigue 38, 75 (2012).
17 R. John, D.J. Buchanan, M.J. Caton, S.K. Jha, Procedia Eng. **2**, 1887 (2010).
18 J.C. Kim, S.K. Cheong, H. Noguchi, Int. J. Fatigue **56**, 114 (2013).
19 Z. Sun, D. Retraint, T. Baudin, A.L. Helbert, F. Brisset, M. Chemkhi, J. Zhou, P. Kanoute, Mater. Charact. **124**, 117 (2017).
20 X.H. Chen, J. Lu, L. Lu, K. Lu, Scripta Mater. **52**, 1039 (2005).

21 J. Petit, L. Waltz, G. Montay, D. Retraint, A. Roos, M. François, Mater. Sci. Eng. A **536**, 124 (2012).
22 J. Oddershede, J.P. Wright, A. Beaudoin, G. Winther, Acta Mater. **85** 301 (2015).
23 Y.J. Wei, L. Anand, J. Mech. Phys. Solids **52** 2587 (2004).
24 Y.J. Wei, A.F. Bower, H.J. Gao, Acta Mater. **56** 1741 (2008).
25 M.A. Meyers, A. Mishra, D.J. Benson, Prog. Mater. Sci. **51** 427 (2006).